The Journal of Veterinary Medical Science

NOTE

Wildlife Science

Detection of squamous cell carcinoma of presumed pancreatic origin and its metastasis in a spotted seal (*Phoca largha*) using ultrasonography and computed tomography

Takeshi TSUKA[1)]*, Tomokazu KOZU[2)], Yuji SUNDEN[1)], Takehito MORITA[1)], Yoshiharu OKAMOTO[1)], Masamichi YAMASHITA[1)], Tomohiro OSAKI[1)], Takao AMAHA[1)], Norihiko ITO[1)], Yusuke MURAHATA[1)] and Tomohiro IMAGAWA[1)]

[1)]Joint Department of Veterinary Medicine, Faculty of Agriculture, Tottori University, Tottori, Japan
[2)]Kinosaki Marine World, Hyogo, Japan

ABSTRACT. A 21-year-old female spotted seal (*Phoca largha*), with a swollen abdomen, had a five-month history of anorexia and vomiting. Ultrasonography revealed an extended mass with central necrotic foci in the right cranial abdomen. Computed tomography revealed an abdominal mass with a low-density central lumen and a pulmonary nodular lesion. Cytology of an abdominal specimen collected through fine-needle aspiration indicated a malignant tumor with round, atypical cells with large nuclei. Three days after diagnosis, necropsy revealed a 10-cm large, solid, whitish mass in the pancreatic parenchyma and multiple small nodules in the liver, spleen, mesentery, lungs, and mediastinal lymph nodes. Histopathological analysis showed prolific neoplastic cells with marked atypia and occasional keratinization. Immunohistochemistry revealed that the neoplastic cells were positive for cytokeratin AE1/AE3 antibody. Thus, the seal was diagnosed with squamous cell carcinoma, of presumed pancreatic origin, which had metastasized to multiple organs.

KEY WORDS: computed tomography, pancreas, spotted seal (*Phoca largha*), squamous cell carcinoma, ultrasonography

J. Vet. Med. Sci.
84(3): 373–377, 2022
doi: 10.1292/jvms.21-0156

Received: 14 March 2021
Accepted: 29 December 2021
Advanced Epub:
20 January 2022

Previous case reports have described tumors originating in various abdominal organs in *Pinnipedia* [6, 7, 10, 13, 14, 17, 23]. Primary lesions in squamous cell carcinomas in *Pinnipedia* have been identified at various locations, including the skin, gingiva, tongue, pharynx, esophagus, lungs, penis, uterus, and vagina [7, 10, 13, 17]. Although the pancreas has rarely been reported as a primary site of abdominal tumors in *Pinnipedia* [14], it has been identified as a distant metastatic organ in a spotted seal (*Phoca largha*) with squamous cell carcinoma [13].

Squamous cell carcinomas have been diagnosed predominantly through postmortem examinations of diseased animals or during necropsy [17]. Ultrasonography, computed tomography (CT), and laparoscopy are used to obtain clinical evidence for selecting either symptomatic or definitive treatment, as illustrated by recent clinical trials involving antemortem diagnosis [2, 3, 7, 17, 22, 23]. This case report describes the clinical applicability of the combined use of ultrasonography and CT to identify squamous cell carcinoma in a spotted seal. Additionally, the histopathological characteristics of the tumor have also been described.

A 21-year-old female spotted seal presented with a swollen abdomen that had gradually developed over the course of six months. The seal lived in an aquarium at Kinosaki Marine World in Hyogo prefecture, Japan. The animal had a five-month history of anorexia and vomiting, resulting in severe weight loss (from 73 to 46 kg). Jugular blood was collected from the seal at admission, and hematological and biochemical parameters were measured and analyzed through a hematology automatic analyzer (pocH-100iV Diff; Sysmex Co., Ltd., Kobe, Japan) and a biochemistry automatic analyzer (DRI-CHEM 7000V; Fujifilm Medical Co., Ltd., Tokyo, Japan), respectively (Table 1). Mild anemia was noted based on the decreased red blood cell count (329 × 10^4/μl) and slightly decreased hematocrit level (33.8%). The white blood cell count was normal (10,600/μl) [4, 18]. The levels of total protein and total cholesterol (9.6 g/dl and 360 mg/dl, respectively) were higher than standard values [4, 18].

*Correspondence to: Tsuka, T.: tsuka@tottori-u.ac.jp, Joint Department of Veterinary Medicine, Faculty of Agriculture, Tottori University, 4-101 Koyama-Minami, Tottori, Tottori 680-8550, Japan

©2022 The Japanese Society of Veterinary Science

This is an open-access article distributed under the terms of the Creative Commons Attribution Non-Commercial No Derivatives (by-nc-nd) License. (CC-BY-NC-ND 4.0: https://creativecommons.org/licenses/by-nc-nd/4.0/)

Table 1. Hematological and serum biochemical values

Variable	This case	Reference range [2]	Reference range [14]
Red blood cell count (×10^4/μl)	329	390–570	390–550
White blood cell count (/μl)	10,600	6,000–14,200	7,500–18,900
Hemoglobin (g/dl)	13.7	13.5–24.0	14.3–22.9
Hematocrit (%)	33.8	35–63	39–62
Total protein (g/dl)	9.6	6.7–8.4	5.7–8.9
Albumin (g/dl)	4.1	-	-
Urea nitrogen (mg/dl)	40.5	22.4–41.5	8.1–35.6
Creatinine (mg/dl)	0.5	0.8–1.3	0.3–1.1
Alkaline phosphatase (U/l)	172	20–84	23–259
Aspartate aminotransferase (U/l)	122	5–91	45–221
Alanine aminotransferase (U/l)	14	6–90	36–69
Total cholesterol (mg/dl)	360	209–321	213–302
Glucose (mg/dl)	161	124–177	87–186
Sodium (mmol/l)	148	147–158	144–156
Chloride (mmol/l)	107	101–112	99–111
Potassium (mmol)	4.5	2.8–4.6	3.9–5.9

For ultrasonographic examination, the animal was sedated using an intramuscular injection of butorphanol tartrate (0.2 mg/kg, Betrorphal; Meiji Seika Pharma Co., Ltd., Tokyo, Japan) and midazolam (0.1 mg/kg, Dormicum; Asteras Pharma Inc., Tokyo, Japan). An ultrasound machine (HI VISION Preirus; HitachiAloka Medical Ltd., Japan) was used to perform an abdominal evaluation. The animal was laid in the left lateral recumbent position, and a 5-MHz microconvex transducer was applied to the right abdomen in conjunction with an ultrasound gel. On sagittal percutaneous scanning, no nodular lesions were apparent within the liver, which appeared as a homogenous echogenic structure extending between the stomach and bladder. Transverse scanning of the right cranial abdomen revealed a smooth, round mass near the distal edge of the liver (Fig. 1a). The mass was approximately 5 cm in diameter and appeared as homogenous hyperechoic mass in the parenchyma compared with the echogenicity of the neighboring hepatic structure. It had a lumen and its center contained anechoic fluid material. The lumen was approximately 3 cm in diameter and was lined by a complete, irregular wall. Doppler ultrasonography revealed less blood flow within the parenchyma of the mass. Soon after the ultrasonographic examination, the animal was placed in the prone position and examined using a 16-section multidetector CT scanner (ECLOS; Hitachi, Tokyo, Japan). Chest CT revealed a 9.3 × 7.4-mm smooth, elliptical nodule in the right caudal pulmonary lobe. In a transverse CT image of the cranial abdomen, a high-density mass (87 × 59 mm) was observed in the space between the stomach on the left and the liver on the right (Fig. 1b). The density of the mass (CT value: approximately 55) was comparatively lower than that of the neighboring hepatic structure. The mass included a homogenous low-density lumen (CT value: approximately 30). The other nodular lesion could not be identified within the abdominal cavity. At this point, the animal had not been examined by contrast CT. Ultrasound-guided fine-needle aspiration was performed using a 22-gauge needle (Terumo spinal needle, Terumo Co., Tokyo, Japan). Cytology of the specimen revealed an accumulation of round, atypical cells with large nuclei, comprising mainly of erythrocytes and neutrophils (Fig. 2a). Based on these findings, a tumor originating in one of the right-side abdominal organs was suspected to be malignant.

Following diagnosis, the animal received symptomatic treatments consisting of sequential intramuscular injections of ampicillin sodium (5 mg/kg; Viccillin, Meiji Seika Pharma Co., Ltd., Tokyo, Japan), glutathione (4 mg/kg; Tathion 200 mg for Injection, Choseido Pharmaceutical Co., Ltd., Tokushima, Japan), and thiamine chloride hydrochloride (0.2 mg/kg; Thiamine chloride hydrochloride injection 10 mg Fuso, Fuso Pharmaceutical Industries, Ltd., Osaka, Japan). However, the animal's condition deteriorated and it died three days after the examinations. Upon necropsy, a 10-cm large, solid, whitish mass was observed within the pancreatic parenchyma (Fig. 1c). The border between the pancreatic parenchyma and protruding mass was clearly visible. The cut surface of the mass appeared to have a cavity surrounded by irregular membranes in the center of the mass. Small nodular formations (2–10 mm in diameter) were observed in the liver, spleen, mesentery, lungs, and mediastinal lymph nodes. Specimens of the pancreas, liver, spleen, mesentery, lungs, and mediastinal lymph nodes were collected and fixed in 10% neutral phosphate-buffered formalin and routinely processed. Paraffin wax-embedded tissues were sectioned into 4 μm thick slices for hematoxylin and eosin staining. Immunohistochemical analysis of pancreatic tissue was performed using a primary antibody for cytokeratin AE1/AE3 (diluted 1:100, Dako, Glostrup, Denmark) with an Envision-labelled polymer reagent, and 3,3′-diaminobenzidine tetrahydrochloride was used as the chromogen. A specificity control was established by replacing the primary antibody with phosphate-buffered saline.

Microscopic examination revealed the proliferation of epithelial neoplastic cells and some inflammatory cells within mass structures connecting pancreatic structures via well-defined fibrous capsules (Fig. 2b). Neoplastic cells were observed to have abundant eosinophilic cytoplasm, along with intercellular bridges between these cells, and occasional keratinization. Many neoplastic cells had prominent nucleoli and some mitotic figures (Fig. 2c). The same neoplastic epithelial cells were also observed in various nests, but with less keratinization in the liver, spleen, mesentery, lungs, and mediastinal lymph nodes. Necrosis of

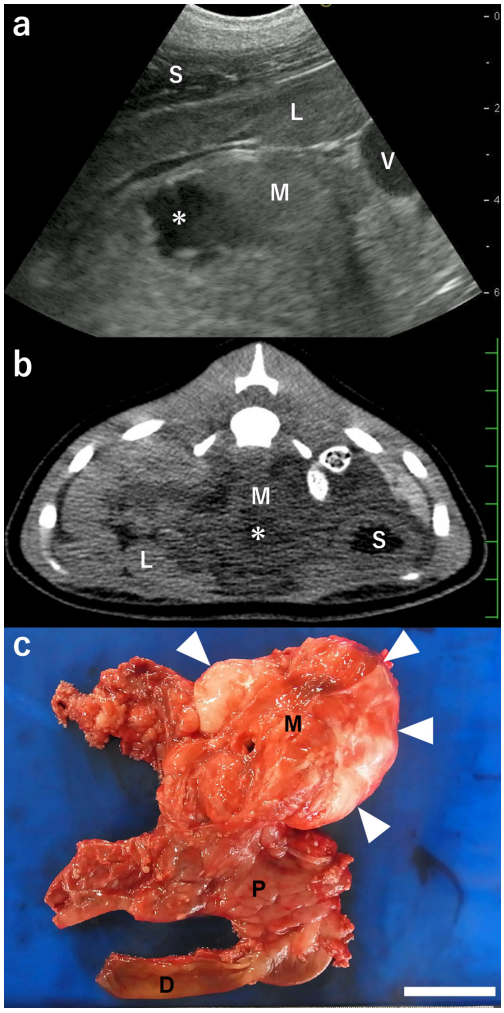

Fig. 1. Ultrasonogram (a), computed tomographic image (b), and macroscopic view (c) of the mass lesion (M) in the pancreas. (**a**) An echogenic mass (M) is seen at sites deeper than the skin, subcutaneous tissues (S), liver (L), and large blood vessels (V). The mass includes a hypoechoic cavity (asterisk) in the center. (**b**) A mass (M) is seen in the space between the stomach (S) and liver (L), and it features a low-density lumen (asterisk) in the center. Scale=25 mm. (**c**) A whitish, round mass (arrowheads) is seen to protrude from the pancreas (P). D, duodenum. Bar=5 cm.

neoplastic cells was occasionally observed in these organs. Furthermore, neoplastic cells showed marked atypia, many mitotic figures (Fig. 2d), and indistinct intercellular bridges (Fig. 2e). The neoplastic cells showed positive immunolabelling for cytokeratin AE1/AE3 (Fig. 2f).

Multiple mass lesions were identified upon antemortem imaging and based on histopathological findings, these lesions were diagnosed as squamous cell carcinoma of presumed pancreatic origin. Metastasis of squamous cell carcinoma was also confirmed based on these findings. The pancreatic lesions were moderately differentiated structures, with evident intercellular bridges and limited keratinization. Lesions found in other organs were poorly differentiated, wherein neither intercellular bridges nor keratinization were evident. Multiple mass formation has been found in *Pinnipedia* with metastatic squamous cell carcinomas [7, 10, 13]. The widespread distribution of affected organs often makes the identification of the primary locus of a tumor difficult [10]. For antemortem identification of these abdominal tumors in marine mammals, various imaging modalities, such as ultrasonography, CT, and endoscopy, can be used [2, 3, 7, 17, 22, 23].

Ultrasonography is commonly used as the first choice for diagnostic imaging in human patients with pancreatic mass formations [1, 5, 11, 12, 24]. However, ultrasonographic findings vary greatly among mass formations in terms of margin irregularity, clarity of the borders between the normal and affected structures (well-defined or ill-defined), echogenicity, homogeneity, and presence or absence of cystic lumens [1, 5, 12]. These variations are also common in the parenchyma of metastatic pancreatic masses [24]. In this study, abdominal ultrasonogram revealed a well-defined, hyperechoic, pancreatic mass with a central anechoic lumen, resembling previously reported ultrasonographic findings in humans [5, 11]. The size of the pancreatic mass measured approximately 9 cm using CT-based examination and 10 cm macroscopically. On the other hand, ultrasonography revealed that mass was approximately 5 cm, especially because an ultrasonogram could not be obtained for the median section of the mass. Our obtained values seemed to be larger in comparison with the CT measurements of masses in human patients [5, 11]. In small animals, pancreatic squamous cell carcinomas appear to be homogenous pancreatic nodules, and nodules that are approximately 2 cm in diameter are suspected to be malignant [8]. Thus, the extension of the lesion might be a specific characteristic of pancreatic squamous cell carcinoma in marine mammals, as the unclear exhibition of clinical signs and delay in diagnosis were the possible causes. However, an accurate diagnosis could not have been obtained prior to the animal's death. Thus, although ultrasonography can provide suggestive evidence for neoplastic or non-neoplastic lesions, it is not useful in determining the origins of the pancreatic lesions [5, 12, 24].

Use of a low-frequency ultrasound transducer (2–5 MHz) is required for ultrasonographic visualization of abdominal masses and deeper abdominal organs in large marine mammals [3, 19], but this may lead to the generation of poor image quality, resulting in misdiagnosis and the overlooking of small pathological changes [23]. In this study, a 5-MHz transducer provided a good view of the pancreatic mass located close to the abdominal wall, but it did not detect the multiple nodules in the liver and spleen.

In previous studies, CT has been utilized for the basic investigation of normal structures [9, 20], and the identification of various diseases [2, 3, 7, 22] in the chest and abdomen of marine mammals. Previous studies have successfully identified esophageal squamous cell carcinomas in two harbor seals using antemortem CT [7]. In human patients, pancreatic squamous cell carcinomas are visualized using CT as large-sized masses with central hypoattenuating foci protruding into pancreatic structures, and these were similar to those found in this study [5, 11, 12]. However, CT findings are commonly suggestive and not diagnostic of squamous cell carcinomas [5, 11, 12]. Primary pancreatic masses cannot be determined based on CT examination because the solitary types of metastatic pancreatic masses are present as large-sized masses with a center foci [16, 21]. Contrast CT can provide complementary information for evaluating malignancy and neovasculature (hypervascularity is a reliable indicator of pancreatic squamous cell carcinoma) based on contrast enhancements of abdominal masses, a technique implemented in human medicine [1, 5, 12, 21]. A previously reported contrast CT procedure [2, 3] could also be helpful for differentiation of abdominal masses in

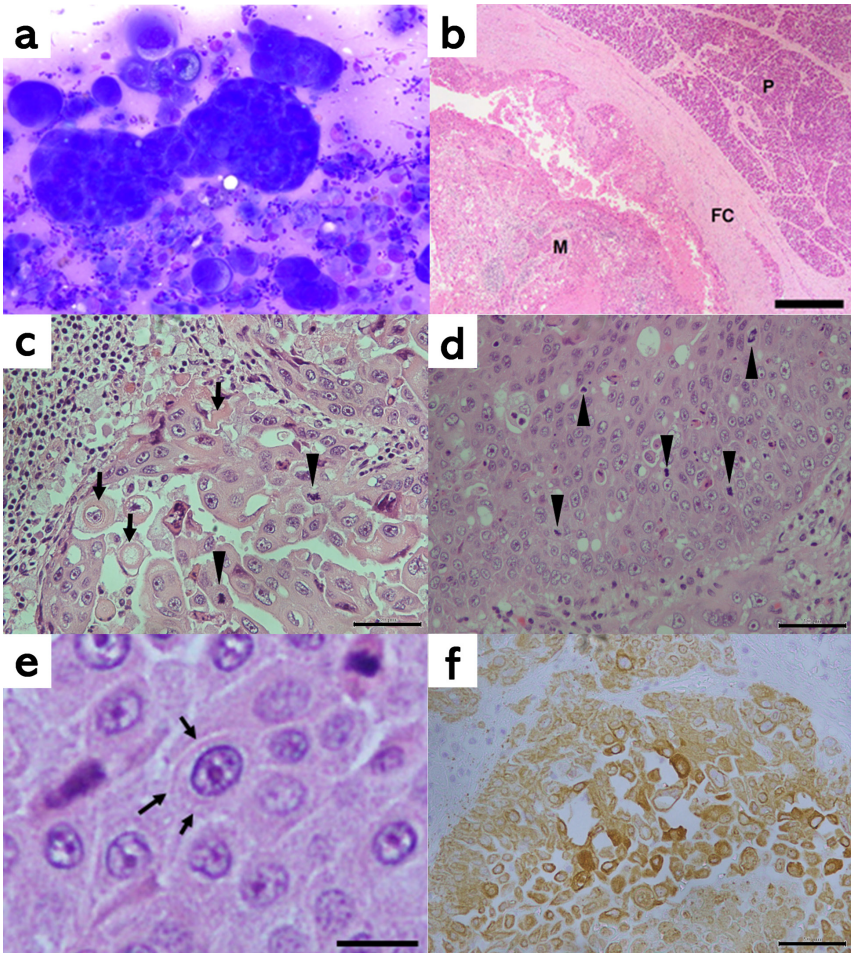

Fig. 2. (**a**) Cytology of a pancreatic mass specimen obtained via ultrasound-guided fine-needle aspiration. Light Giemsa stain. (**b**) Low-magnification histopathological view of the mass (M) and pancreas (P). Proliferation of epithelial neoplastic cells with eosinophilic debris and some inflammatory cells are evident. Infiltration of some neoplastic cells occurs within the fibrous capsules (C). Hematoxylin and eosin stain. Bar=500 µm. (**c**) High-magnification histopathological view of the pancreatic mass. Neoplastic cells occasionally show keratinization (arrows) and mitotic figures (arrowheads). Bar=50 µm. (**d**) High-magnification histopathological view of the mediastinal lymph node. The neoplastic cells show marked atypia and many mitotic figures (arrowheads). Bar=50 µm. (**e**) High-magnification histopathological view of the mediastinal lymph node. The neoplastic cells sometimes show intercellular bridges (arrows). Bar=10 µm. (**f**) High-magnification immunohistochemical view of the pancreatic mass. The neoplastic cells are immunopositive for cytokeratin antibody (AE1/AE3). Bar=50 µm.

marine mammals, although it was not used in this case.

CT is also suitable for detecting systemic metastasis, which is indicated by mass lesions extending into multiple body cavities [16, 24]. However in this study, CT did not help in visualizing nodules embedded in the liver and the spleen or the anatomical continuity between the large mass and the pancreas. This may also be due to the thick layer of blubber surrounding the abdomen in pinnipeds, thereby leading to poor contrast in abdominal CT images [3, 20]. Poor imaging quality also hampered the visualization of mass formation within the pancreas. Prolonged scanning time in CT, especially in large animals, can result in blurred images because of cyclic body movements that occur due to respiration in animals [15]. CT visibility may be improved in anesthesia which causes controlled respiratory arrest via tracheal intubation [2, 3, 15]. Compared to the CT machine (16-slice) used in this study, the use of a multi-detector (>16-slice) CT scanner with a shorter scanning time may provide higher quality images [9].

Ultrasonography enables real-time observation of abdominal tumors in marine mammals [16]. Unlike CT, wherein anesthesia is required for antemortem examination [6, 7], the use of sedation and anesthesia is not strictly necessary for performing percutaneous ultrasonography in marine mammals [19] Thus, ultrasonography is superior to CT for routine examination given that it can be performed without sedation and anesthesia. In addition, ultrasonographic visualization can help guide procedures like percutaneous abdominocentesis, which in this case study provided evidence of an abdominal tumor. CT can be utilized as a supplemental imaging modality, allowing full body evaluations and accurate measurement of size and degree of vascularity while diagnosing mass lesions. Combined use of these diagnostic techniques is expected to elevate antemortem diagnostic accuracy for abdominal tumors in marine mammals.

POTENTIAL CONFLICTS OF INTEREST. The authors have nothing to disclose.

REFERENCES

1. Abedi, S. H., Ahmadzadeh, A. and Mohammad Alizadeh, A. H. 2017. Pancreatic squamous cell carcinoma. *Case Rep. Gastroenterol.* **11**: 219–224. [Medline] [CrossRef]
2. Dennison, S. E., Van Bonn, W., Boor, M., Adams, J., Pussini, N., Spraker, T. and Gulland, F. M. D. 2011. Antemortem diagnosis of a ventricular septal defect in a California sea lion *Zalophus californianus*. *Dis. Aquat. Organ.* **94**: 83–88. [Medline] [CrossRef]
3. de Swarte, M., Bryan, J., Zarelli, M., Huuskonen, V., Schneeweiss, W. and McAllister, H. 2013. Imaging diagnosis-ultrasonographic and CT findings in a gray seal (*Halichoerus grypus*) with hepatic cirrhosis, pyelonephritis, and nephrolithiasis. *Vet. Radiol. Ultrasound* **54**: 555–559. [Medline] [CrossRef]
4. de Swart, R. L., Ross, P. S., Vedder, L. J., Boink, F. B. T. J., Reijnders, P. J. H., Mulder, P. G. H. and Osterhaus, A. D. M. E. 1995. Haematology and clinical chemistry values for harbour seals (*Phocavitulina*) fed environmentally contaminated herring remain within normal ranges. *Can. J. Zool.* **73**: 2035–2043. [CrossRef]
5. Fajardo, L. L., Yoshino, M. T. and Chernin, M. M. 1988. Computed tomography findings in squamous cell carcinoma of the pancreas. *J. Comput. Tomogr.* **12**: 138–139. [Medline] [CrossRef]
6. Fauquier, D., Gulland, F., Haulena, M. and Spraker, T. 2003. Biliary adenocarcinoma in a stranded northern elephant seal (*Mirounga angustirostris*). *J. Wildl. Dis.* **39**: 723–726. [Medline] [CrossRef]
7. Flower, J. E., Gamble, K. C., Stone, M., Lyons, J. A., Maganti, R. J., Tuomi, P. A., Olds, J. E., Sims, M. A., Gauger, P. and Tuttle, A. D. 2014. Esophageal squamous cell carcinoma in six harbor seals (*Phoca vitulina* spp.). *J. Zoo Wildl. Med.* **45**: 620–631. [Medline] [CrossRef]
8. Hecht, S. and Henry, G. 2007. Sonographic evaluation of the normal and abnormal pancreas. *Clin. Tech. Small Anim. Pract.* **22**: 115–121. [Medline] [CrossRef]
9. Ivančić, M., Solano, M. and Smith, C. R. 2014. Computed tomography and cross-sectional anatomy of the thorax of the live bottlenose dolphin (*Tursiops truncatus*). *Anat. Rec. (Hoboken)* **297**: 901–915. [Medline] [CrossRef]
10. Joseph, B. E., Cornell, L. H. and Migaki, G. 1986. Metastatic squamous cell carcinoma in a beached California sea lion (*Zalophus californianus*). *J. Wildl. Dis.* **22**: 281–283. [Medline] [CrossRef]
11. Kashani, A., Kahn, M. and Jamil, L. H. 2015. Diagnosis of primary squamous cell carcinoma of the pancreas using endoscopic ultrasound-guided core needle biopsy. *Gastroenterol. Rep. (Oxf.)* **5**: 72–74. [Medline] [CrossRef]
12. Lai, L. H., Romagnuolo, J., Adams, D. and Yang, J. 2009. Primary squamous cell carcinoma of pancreas diagnosed by EUS-FNA: a case report. *World J. Gastroenterol.* **15**: 4343–4345. [Medline] [CrossRef]
13. Michishita, M., Torikai, K., Yoshimura, H., Terasawa, F., Nakahira, R., Ohkusu-Tsukada, K. and Takahashi, K. 2013. Squamous cell carcinoma with systemic metastases in a spotted seal (*Phocalargha*). *Jpn. J. Zoo Wildl. Med.* **18**: 129–132. [CrossRef]
14. Moore, J. J. and Stackhouse, L. L. 1978. Pancreatic duct adenoma and strangulation of the small intestine in a California sea lion (*Zalophus californianus*). *J. Wildl. Dis.* **14**: 445–446. [Medline] [CrossRef]
15. Morita, Y., Sugiyama, S., Tsuka, T., Okamoto, Y., Morita, T., Sunden, Y. and Takeuchi, T. 2019. Diagnostic efficacy of imaging and biopsy methods for peritoneal mesothelioma in a calf. *BMC Vet. Res.* **15**: 461. [Medline] [CrossRef]
16. Muranaka, T., Teshima, K., Honda, H., Nanjo, T., Hanada, K. and Oshiumi, Y. 1989. Computed tomography and histologic appearance of pancreatic metastases from distant sources. *Acta Radiol.* **30**: 615–619. [Medline] [CrossRef]
17. Newman, S. J. and Smith, S. A. 2006. Marine mammal neoplasia: a review. *Vet. Pathol.* **43**: 865–880. [Medline] [CrossRef]
18. Roletto, J. 1993. Hematology and serum chemistry values for clinically healthy and sick pinnipeds. *J. Zoo Wildl. Med.* **24**: 145–157.
19. Seitz, K. E., Smith, C. R., Marks, S. L., Venn-Watson, S. K. and Ivančić, M. 2016. Liver ultrasonography in dolphins: Use of ultrasonography to establish a technique for hepatobiliary imaging and to evaluate metabolic disease-associated liver changes in bottlenose dolphins (*Tursiops truncatus*). *J. Zoo Wildl. Med.* **47**: 1034–1043. [Medline] [CrossRef]
20. Smodlaka, H., Henry, R. W., Daniels, G. B. and Reed, R. B. 2004. Correlation of computed tomographic images with anatomic features of the abdomen of ringed seals (*Phoca hispida*). *Am. J. Vet. Res.* **65**: 1240–1244. [Medline] [CrossRef]
21. Tan, C. H., Tamm, E. P., Marcal, L., Balachandran, A., Charnsangavej, C., Vikram, R. and Bhosale, P. 2011. Imaging features of hematogenous metastases to the pancreas: pictorial essay. *Cancer Imaging* **11**: 9–15. [Medline] [CrossRef]
22. Weisbrod, T. C., Walsh, M. T., Marquardt, S. and Giglio, R. F. 2020. Computed tomography diagnosis of pneumothorax and cardiac foreign body secondary to stingray injury in a Bottlenose dolphin (*Tursiops truncatus*). *Aquat. Mamm.* **46**: 326–330. [CrossRef]
23. Yamazaki, M., Koutaka, M. and Une, Y. 2016. Gastric carcinoma in a South American sea lion (*Otaria flavescens*). *J. Vet. Med. Sci.* **78**: 1201–1204. [Medline] [CrossRef]
24. Yoshinaga, S., Suzuki, H., Oda, I. and Saito, Y. 2011. Role of endoscopic ultrasound-guided fine needle aspiration (EUS-FNA) for diagnosis of solid pancreatic masses. *Dig. Endosc.* **23** Suppl 1: 29–33. [Medline] [CrossRef]